Clinics of Oncology

Research Article ISSN: 2640-1037 |Volume 8

A prospective pilot analysis of Correlation of F-18 FDG PET/CT Radiomics with Tumor Mutations from Cell free DNA in Lung Cancer Patients

Nejabat M[1]*, Leisser A[1], Papp L[2], Spielvogel CP[1,4], Streubel B[3], Vraka C[1], Prosch H[5], Karanikas G[1], Hacker M[1], Kenner L[3,4] and Haug A[1,4]

[1]Department of Biomedical Imaging and Image-guided Therapy, Division of Nuclear Medicine, Medical University of Vienna, Austria

[2]QIMP group, Center of Medical Physics and Biomedical Engineering, Medical University of Vienna

[3]Department of Pathology, clinical institute for Pathology, Medical University of Vienna, Austria

[4]Christian Doppler Laboratory for Applied Metabolomics (CDL AM), Medical University of Vienna

[5]Department of Biomedical Imaging and Image-guided Therapy, Division of General and Pediatric Radiology, Medical University of Vienna, Austria

***Corresponding author:**

Alexander Haug,
Department of Biomedical Imaging and Image-guided Therapy, Division of Nuclear Medicine, Medical University of Vienna, Austria

Received: 26 Oct 2024
Accepted: 12 Nov 2024
Published: 16 Nov 2024
J Short Name: COO

Citation:

Haug A, A prospective pilot analysis of Correlation of F-18 FDG PET/CT Radiomics with Tumor Mutations from Cell free DNA in Lung Cancer Patients.
Clin Onco. 2024; 8(4): 1-17

1. Abstract

F-18 FDG PET/CT imaging radiomics and cell free DNA (cfDNA) analysis also known as liquid biopsy are both gaining interest for characterization of tumors in personalized cancer therapy. Both are minimal invasive, widely availability and feasible. Aim of this study was to examine the correlation of the F-18 PET/CT radiomics with the lung cancer mutations from cfDNA.

1.1. Methods: Fifty-five lung cancer patients were prospectively recruited. Radiomics feature extraction from F-18 FDG PET/CTs as well as genome mutation analysis of cfDNA for lung cancer relevant mutations such as RET, EGFR, KDR, HRAS, SKT11, ERRB4, FGFR and PIK3CA from the same patients at the same time point were performed. Tumor volume (TV) and total lesion glycolysis (TLG) were defined by volumetric PET parameters. Patient's survival was analyzed according to the tumor volume and different radiomic features. Present mutations were correlated with extracted radiomic features.

1.2. Results: We found significant relationships between multiple features in PET/CT radiomics and mutated genes in cfDNA. The most significantly correlated features were related to homogeneity of the tumor in terms of structure as well as metabolism. A number of CT, PET and fusion PET/CT features correlated with mutations in cfDNA: PET GLCM Dissimilarity for SKT 11 (AUC=0.80; P< 0.0001), CT Histogram Entropy for FGFR mutation (AUC=0.86; P<0001), CT Intensity Mean for EGFR (AUC=0.72; P=0.0167), PET Histogram Entropy for PIK3CA (AUC=0.77; P= 0.0002) and CT Histogram Kurtosis for RET mutation (AUC=0.74; P<0.0001). Tumor volume, and TLG significantly correlated with survival (P-Value: 0.04 and 0.04, respectively). A decision tree model applied using the two radiomic features with the highest AUC correlates with the prevalence of mutations. For FGFR, the prevalence of mutation increased from 5% to 50% and 90% for score zero, score one and score two, respectively. In conclusion, the most important and new finding of this study is the significant correlation of several FDG PET/CT radiomic features with relevant mutations from cfDNA in lung cancer. These findings might help to characterize lung cancer, it's residue after treatment or recurrence non-invasively, and potentially accurate (with the combination of liquid biopsy and radiomics) with impact on treatment.

2. Introduction

Tumor heterogeneity is an important principle not only per patient but also in different stages of disease in cancer patients. Genome wide association studies are increasingly used as appropriate and important tool in the development of personalized therapy in can-

cer patients (verma, 2017). As biopsies are invasive and prone to sampling error, a non-invasive tumor characterization such as liquid biopsy, which can be repeated easily in different stages of disease, is needed.

Liquid biopsy is considered as a minimally invasive method which has the potential to be used for detecting tumor derived markers for diagnostic and prognostic purposes (Siravegna, 2019). In recent years, several studies have evaluated the validity of liquid biopsy in diagnosis, prognosis and follow-up of multiple cancers (Cohen, 2017).

Per definition, circulating extra nuclear nucleic acids – including cell free DNA (cfDNA) - are considered as one subgroup of liquid biopsies which carries information about the dynamics of cancer specific gene alterations. (Volik, 2016) A study with colon cancer patients showed that the amount of cfDNA in the blood is correlated with patients' outcome. (Boysen, 2017) Other results point towards a possible monitoring of cfDNA level for prolonging the period of follow-up images like computed tomography. (Bi, 2020) (Lyskjær, 2019)

The importance of tumor specific gene mutations on therapy response is well established. The association between cfDNA and clinical outcome, invasiveness of the tumor or clinical response is already studied to some extent (Boysen a. k., 2017). Several studies have shown the correlation of mutations analyzed from cfDNA and tissue samples (Herbreteau, 2019). In lung cancer patients, recently multiple studies reported the concordance of EGFR mutation in plasma and tissue samples of non-small cell lung cancer (NSCLC) patients. (Liu1†, 2020) (Ianza, 2021) (Ntzifa, 2021) .

Another non-invasive approach for characterization of cancer is the use of radiomics. In radiomics-based studies a large number of features, extracted from medical in vivo images, are used to identify cancer-specific imaging signatures, which may correlate with the biology of cancer cells. (Hong, 2020)

Deregulation of cellular energy metabolism is a hallmark of cancer, which is why FDG-PET is used to image cancer clinically (Pavlova, 2016). There is growing evidence, that FDG uptake by tumors is altered by driver oncogenes, while oncogene downregulation results in decreasing FDG uptake, preceding effects on tumor regression. (Alvarez, 2014) (Heiden, 2018)

We hypothesize that activated oncogenic pathways within a tumor are a primary determinant of its metabolism and provide a framework to interpret effects on this key parameter in clinical imaging. We tried to identify distinct phenotypic metabolism patterns via PET/CT radiomic-based characteristics and correlated it with gene expression data from cfDNAs of the same lung cancer patients.

3. Materials and Methods

3.1. Study Design and Patient Selection: This study was performed as a single center, prospective cohort study, starting in 2016 after IRB approval (ethics approval number 1649/2016) until 2018. Lung cancer patients, regardless of the histological type of cancer (adeno carcinoma, squamous cell carcinoma etc.) and also regardless of the cancer staging situation (primary or metastatic) scheduled for 18F-FDG PET/CT imaging at the Division of Nuclear Medicine of the University Hospital in Vienna have been included in our study.

An informed consent was signed by both competent physician and patient after a detailed information. Patients who have had an ongoing therapy at the time of PET imaging and those who had any acute parallel inflammatory process or medical procedure which may affect PET-uptake (recent operation, second malignancy, acute infection, known inflammatory disease) were excluded from the study.

Relevant information including histopathological data and/or cytology data (if present) of each patient was collected from the IT system of Vienna general hospital [AKH-Information Management (AKIM)].

3.2 Isolation and Quantification of Cell-Free DNA from Blood Samples: Peripheral blood from included patients was collected in cell-free DNA collection tubes (Streck) before the application of 18F-FDG. Blood samples were proceeded within 12 hours of collection via a 2-step centrifugation protocol. Plasma was separated from the other blood components by centrifugation at 2000-x g for 20 minutes at 22°C. After transferring the upper plasma layer to a new conical tube, it was centrifuged at 3200-x g for 30 minutes at 22°C to remove cell debris. Subsequently the resulting plasma supernatant was stored at -20°C until cfDNA isolation. Circulating DNA isolation from 5-10ml plasma was performed on the Chemagic 360 Instrument (Perkin Elmer) with the isolation kit CMG-1111 (Chemagic cfDNA 10k Kit special H12) according to manufacturer's instruction. Cell-free DNA was eluted in 50µl Elution Buffer. DNA quantification was performed with Qubit® dsDNA HS Assay Kit (Invitrogen) according to the instructions provided by the manufacturer and purity was determined by Agilent 2200 TapeStation System. Cell-free DNA was stored at -20°C until further analysis.

3.3 Next-Generation Sequencing (NGS) of cell-free DNA: Library preparation was conducted using AmpliSeq™ Library PLUS with AmpliSeq™ Cancer HotSpot Panel v2 for Illumina®. This panel is designed to amplify 207 amplicons covering hotspot regions of 50 genes with known association to cancer. (Supplementary Table 1) Subsequent sequencing of pooled libraries was performed in several runs on the MiniSeq Illumina platform using MiniSeq High Output Reagent Kit (300-cycles). Data analysis was conducted using DNA Amplicon workflow via Base space Sequence Hub. The NGS data alignment was performed with Burrows-Wheeler Aligner (BWA) and subsequently Somatic Variant Caller was used. Variant annotation was performed with Illumina VariantStudio 3.0 Software. RET, EGFR, KDR, HRAS, PIK3CA, SKT11, ERRB4 and FGFR were determined for the analysis.

Table 1: Mutations identified in cfDNA by use of next generation sequencing (N=20)

Gene	dbSNP	Protein	Coverage	Alt variant frequency (%)	Allele frequency (%)
ALK	rs3738868	NM_004304.4.3594C>T(p.=)	38884	48.3	10.3
EGFR,EGFRAS1	rs1050171	NM_005228.3.2361G>A(p.=)	2247	51.3	43.27
CDKN2A	rs774904310		2198	3.1	0.3
CSF1R	rs547653185		4299	47.9	0.3
ERBB4	rs839541	NP_005226.1.Tyr283Ter	5097	45.8	35.5
FGFR1		NP_001167538.1.Thr297Ile	47	14.9	0.5
FGFR3	rs3135898	NM_001163213.1.1965+22G>A	5755	52.3	2.12
FLT3	rs75580865	NM_004119.2.2053+23A>G	3993	84.1	3.07
HRAS	rs12628	NM_005343.2.81T>C(p.=)	5417	52.4	29.71
IDH1	rs11554137	NM_005896.2.315C>T(p.=)	7883	51.6	5.69
JAK3	rs3213409	NP_000206.2.Val722Ile	3231	51.5	0.36
KDR	rs7692791	NP_002244.1.Gln472His	2610	55.2	54.41
KIT	rs3822214	NM_000222.2.1638A>G(p.=)	4762	51.8	6.45
KRAS	rs121913529	NP_203524.1.Gly12Val	8584	32.8	0.8
MET	rs56391007	NP_001120972.1.Arg359Gln	3143	52.2	0.34
PDGFRA	rs2228230	NM_006206.4.2472C>T(p.=)	3812	50.5	24.04
PIK3CA	rs3729674	NM_006218.2.3075C>T(p.=)	796	50.9	27.34
RET	rs1800861	NM_020975.4.2307G>T(p.=)	5263	48.8	71.25
SMAD4	rs948588	NM_005359.5.354G>A(p.=)	4083	48.7	3.87
SMARCB1	rs5030613	NM_003073.3.1119-41G>A	30.73	46.4	15.18
STK11	rs2075606	NP_000446.1.Phe354Leu	1898	55.3	35.96
TP53	rs1800372	NM_000546.5.639A>G(p.=)	4886	48.7	0.54

3.4 Imaging protocol: Whole-body 18F-FDG PET/CT from mid cranium to the upper thighs was performed using a 64-row, multi-detector PET/CT system (Biograph™

TruePoint™ 64; Siemens Healthineers, Erlangen, Germany) with an axial fieldof-view of 216 mm, a PET sensitivity of 7.6 cps/kBq, and a transaxial PET resolution of 4–5 mm (full-width at half-maximum, FWHM).

Prior to imaging, patients fasted for 6 hours; the blood glucose cut-off level was 150 mg/dl. PET images were obtained at 50-60 min after the intravenous administration of an average dose of 300 MBq (range: 275-320 MBq) of 18FFDG, over 5-6 bed positions (bp) and an emission scan of 2-3 min per bp. PET images were reconstructed using the Siemens TrueX algorithm, with 4 iterations and 21 subsets, a 5 mm slice thickness and a 168x168 matrix. Venous-phase CECT was performed following the intravenous injection of 100 ml Iomeron 300 (Bracco, Milan Italy) at a rate of 2 ml/s, followed by a 50 ml saline flush and CT with the following parameters: a tube current of 120 mA, a tube voltage of 230 keV, a collimation of 64x0.6 mm, a slice thickness of 3 mm with 2 mm increments and a 512x512 matrix.

3.5 Primary Image Analysis and Tumor Segmentation: A nuclear medicine physician assessed the PET/CT fusion of each case visually for correct alignment, and if necessary, co-registered the images manually by applying Hermes Hybrid 3D Viewer (Hermes Medical Solutions, Stockholm, Sweden). The collected PET CT images were delineated by using the standard isocount 3D VOI (Volume of Interest) generation tool of the Hermes Hybrid 3D software (Hermes Medical Solutions, Stockholm, Sweden) using a correlated threshold of each patients imaging with the average of 3,12 for Tumor lesion glycolysis (TLG) and metabolic tumor volume (MTB) were calculated for all tumor lesions (metastatic and primary) according to the known protocol (Im, 2013). From CT VOIs, Hounsfield Units (HU) were extracted. A reference standard uptake value (SUV) threshold was given for each lesion serving as stopping criteria of the 3D isocontour generation. If necessary, manual modification of the isocontour threshold was performed. In addition, manual slice-by-slice VOI boundary modification was done for proper delineation of each lesion. A reference region (liver) also has been defined for calculation of tumor-tobackground ratio (TBR). The delineated regions were saved to PACS into the project folder. (Figure 1)

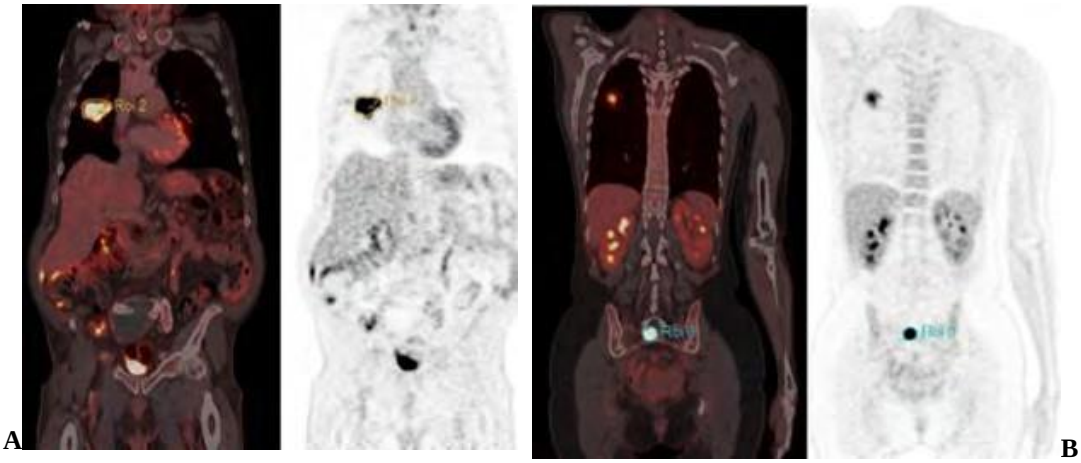

Figure 1: Coronal view of two example fused PET/CT images (left) and PET images (right) from the lung cohort in coronal. A patient with primary lung cancer B patient with primary and metastatic lung cancer.

3.6 Quantitative Image Feature Extraction: The primary endpoint of the study was to investigate if radiomic features extracted from PET/CT imaging correlate with the results of cfDNA gene analysis. Therefore, VOIs were exported to comma-separated value (CSV) file formats from the Hybrid 3D software. Calculation of 90 conventional as well as textural parameters has been performed over the 3D arrays (See supplemental Table 1 as of IBSI guidelines).

Establishment of a feature vector database: All extracted features (Supplement Table 1) were stored in a feature vector database in a row together with the respective mutation mask extracted from the cfDNA of the same patient. The resulting database was saved in a standard CSV file. Each row contains PET, CT and fused PET/CT features together with the analyzed gene mutations.

3.7 Statistical Analysis: Extracted data including patient's radiomic and genomic information expressed with mean and standard deviation as quantitative variables whereas age, sex and gene mutation data used as categorical independent variables. We tested for survival differences in patients with mutated versus non-mutated genes with the Kaplan-Meier analysis using log-rank test. The correlation between tumor volume and/or TLG with survival rate also was done with the Kaplan-Meier analysis using log-rank test. The Wilcoxon (Mann-Whitney U) range sum test was used to determine whether there is a significant difference in each imaging feature value with specific mutated cases versus non-mutated ones (as an example measurement of tumor-to-background ratio as a quantitative feature have been checked in EGFR mutated ones versus non-mutated group). A p-value less than 0.05 was considered as significant. For each statistically significant feature per specific mutation, we evaluated the predictive value of the feature for the correlated mutation using the area under curve (AUC) receiver-operating characteristic (ROC analysis). Analysis and curves were performed using PrismGraphPad and Statistical Package for Social Science (SPSS version 25).

3.8 Data policy: All patients have been pseudonymized for further evaluation. Only authorized persons have had access to the data. The data was stored on a PC with access restrictions.

4. Results

4.1 Patient characteristics: From 55 liquid biopsies and PET CTs taken from lung cancer patients, 41 samples/images were used for further evaluations. 14 samples had to be excluded because of blood lysis, lack of obtained plasma for detecting cfDNA or inappropriate imaging quality.

Clinical characteristics of the studied patients are presented in (Table 1), including the type of cancer, indication for imaging at the time of liquid biopsy (primary staging, therapy response, follow up, post-operative, etc.) and accessibility of pathology tissue from the primary tumor. For all available pathology tissuesections from studied patients with adenocarcinoma and squamous cell carcinoma EGFR was tested routinely. Pathology tissues obtained since 2018 have been tested additionally for ALK, ROS, KRAS, TP53 and PIK3CA mutation as well as a routine procedure. From 41 patients, 32 (78%) had a pathology report from primary tumor and in 6 patients the time interval between tissue biopsy and liquid biopsy was less than 40 days. 75% of patients were diagnosed with non-small cell lung cancer (NSCLC) with 70% was adenocarcinoma (ADC), 21% squamous cell carcinoma (SCC) and 9% other types. Sex and age also followed a normal distribution pattern with male dominancy in SCC and female dominancy in ADC and higher prevalence in elderly. (Kabir, 2008) (Sagerup1, 2011)

Table 1: Clinical characteristic of patients

Patients	Total	ADC	SCC	SCLC	Carcinoid	Others
Male	24	10	6	3	1	4
Female	17	12	3	0	2	0
Age > 65	27	15	5	2	2	3
Age < 65	14	9	4	1	0	0
Tumor Situation at the Time of Liquid Biopsy						
Primary Tumor	7	4	1	2	0	0
Post-operative +/- CHT	11	7	4	0	0	0
CHT +/- Radiation	23	11	5	1	3	3
Available Primary Tumor Pathology	32	20	7	1	3	1

ADC: Adenocarcinoma; **SCC**: Squamous Cell Carcinoma; **SCLC**: Small Cell Carcinoma; **NET**: Neuroendocrine Tumor; **Others**: Sarcoma, Melanoma; **CHT**: Chemotherapy

4.2 Detection gene mutation in fcDNA: cfDNA isolation and sequencing was successful in all included patients. A list of detected mutations in cfDNA with percentage of allele frequency, coverage and all important gene information is given in (Supplementary Table 1). All studied patients have had at least one detected mutation. As shown in (Figure 2), 22 germline mutations were detected in cfDNA of cancer patients. RET, KDR and EGFR had the highest percentage of mutations in the study population with 84%, 82% and 77%, respectively.

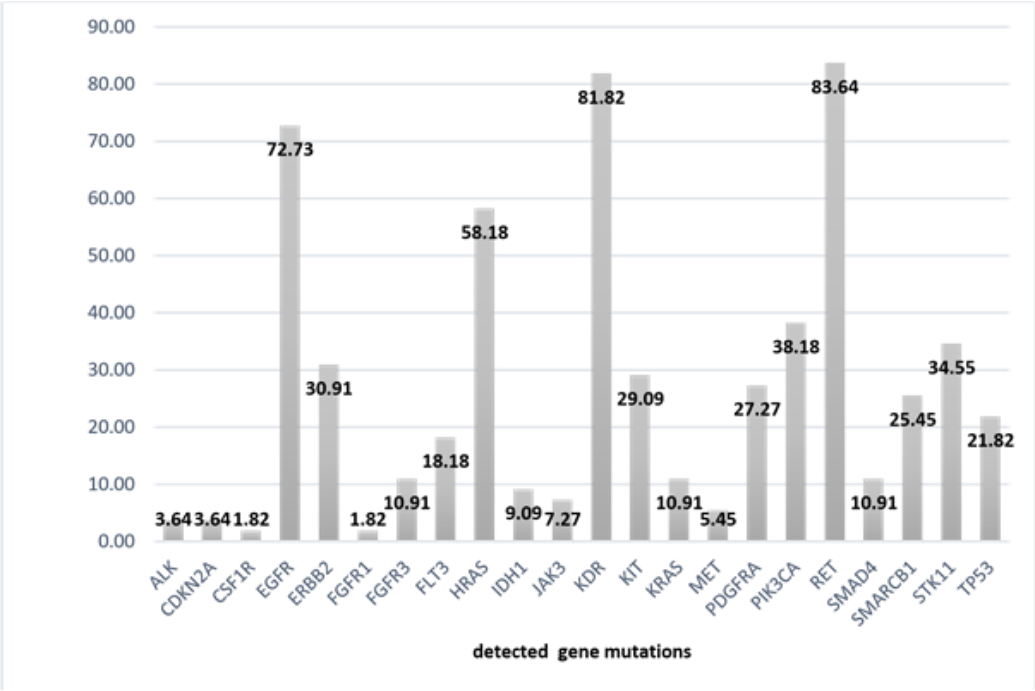

Figure 2: Percentage of detected different mutations in liquid biopsy (cfDNA) of lung cancer patients. Genes are alphabetically arranged; figure is produced by Microsoft excel.

4.3 Correlation of Mutated genes in cfDNA with Radiomic Features: There was no correlation between the number of mutations per patient and TLG. A significant correlation was detected between tumor volume and TLG -as two separate independent factors- with mortality in the study population. (p-value: 0.04 & 0.04). From approximately 90 radiomic features which were extracted from F-18 FDG PET-CT images, after using a feature selection method for reducing redundancy, 50 features remained as main features for further evaluation. (Figure 3) shows the correlation heat map with radiomic features before and after redundancy reduction. In the next step each mutated gene was analysed with any of chosen extracted features statistically for possible correlation. (Table 2) and (Figure 4) are showing the features which significantly correlated with presence or absence of mutation in any of above-mentioned genes. (Significant p-value considered as <0.05).

Table 2 shows that overall more PET features correlated significantly with different cfDNA mutations than CT features (25 vs. 15). We had also 8 fusion features (PET-CT fusion features) cor-

relating with various cfDNA mutations. Looking at each gene mutation separately, RET and SKT11 mutation had the highest number of correlated features (Table 2) and SKT11 had the strongest correlation with average p-value of 0.007 with different radiomics (Table 2). Color plot curve shows that the HRAS, KDR and SKT 11 have had the highest number of correlating radiomic features. (Table 2 and Figure 4).

(Figure 5) displays exemplary results of important fusion PET-CT features (Figure 5/A), CT (Figure 5/B), and PET (Figure 5/C) in different cfDNA mutations separately. The most commonality between different mutations and radiomics was observed in "PET-CT fusion: Inverse difference", which is a feature connected to the homogeneity of tumor, (Figure 5/A) which is significant in 4 genes. Among CT related features "CT GLCM cluster prominence", which shows the symmetry of distribution in measure area of tumor correlated to RET, FGFR and SKT11 mutation (Figure 5/B). In the PET related features, "PET GLCM Cluster shade" had a significant correlation with 5 mutated genes (Figure 5/C) and "PET GLCM difference entropy" and "PET GLCM dissimilarity", each showed correlation with 4 mutated genes.

Table 2: Radiomic features which statistically correlated with detected cfDNA mutation separated by gene. Calculation is done by Mann-Whitney Test (P Value<0.05 considered as significant)

HRAS	**p-Value**	**RET**	**P-Value**
CT::Intensity::Maximum	0.0089	CT::Histogram::Kurtosis	0.0001
CT::NGTDM::Coarseness	0.0341	CT::Histogram::Mean	0.0414
CT::Histogram::Energy	0.0106	CT::Intensity::Sum	0.0449
CT::GLZSM::Large zone low gray Emphasis	0.0419	CT::GLCM::Cluster prominence	0.0084
CT::NGTDM::Texture strength	0.012	CT::GLCM::Entropy	0.0154
PET::GLZSM::Large zone size emphasis	0.0481	CT::GLCM::Sum variance	0.0025
PET::Histogram::Energy	0.0063	PET::GLCM::Dissimilarity	0.0015
PET::Histogram::Kurtosis	0.0037	PET::GLCM::Difference entropy	0.0055
PET::Histogram::Skewness	0.0015	PET::NGTDM::Contrast	0.0012
PET::GLZSM::Small zone size emphasis	0.0136	PET::Intensity::Mean	0.0414
PET+CT::Fusion::Normalized mutual info	0.0022	PET::GLCM::Cluster shade	0.0134
PET+CT::Fusion::Correlation	0.049	PET::GLZSM::High gray level zone emphasis	0.0107
		PET::GLCM::Sum of squares variance	0.0078
		PET::Histogram::Mean	0.0208
		PET::Histogram::Variance	0.0162
		PET::Intensity::Maximum	0.0243
		PET::GLCM::Inverse difference moment	0.0023
		PET::GLCM::Sum average	0.0068
		PET+CT::Fusion::Inverse difference	0.0017
EGFR	P-Value	ERBB4	P-Value
CT::Histogram::Kurtosis	0.0186	PET+CT::Fusion::Inverse difference	0.0268
CT::Histogram::Mean	0.0155	CT::NGTDM::Coarseness	0.0417
CT::Intensity::Sum	0.023		
CT::Intensity::Mean	0.0155		
PIK3CA	P-Value	FGFR	P-Value
PET::GLCM::Cluster shade	0.0017	CT::Histogram::Entropy	<0.0001
PET::Histogram::Entropy	<0.0001	CT::GLCM::Cluster prominence	0.0452
PET::NGTDM::Contrast	0.0083	PET+CT::Fusion::Inverse difference	<0.0001
PET::GLCM::Difference entropy	0.0055	PET::GLCM::Cluster shade	0.0071
PET::GLCM::Sum average	0.0265	PET::GLCM::Inverse difference	0.0025
PET::GLCM::Inverse difference moment	0.0117	PET::GLCM::Sum average	0.0028
PET::GLCM::Dissimilarity	0.0027	PET::NGTDM::Contrast	0.0427
PET::GLZSM::Large zone high gray emphasis	0.0147	PET::GLCM::Dissimilarity	0.0049
PET::NGTDM::Complexity	0.0174	PET::GLCM::Sum Entropy	0.0152
PET::NGTDM::Texture strength	0.0042	PET::GLZSM::Large zone high gray emphasis	0.0026

		PET::NGTDM::Complexity	0.0115
		PET::NGTDM::Texture strength	0.005
SKT11	P-Value	KDR	P-Value
CT::Histogram::Entropy	0.0034	CT::GLCM::Angular second moment	0.0178
CT::GLCM::Cluster prominence	0.019	CT::GLCM::Entropy	0.0262
CT::GLCM::Sum variance	0.0065	PET+CT::Fusion::Inverse difference moment	0.0339
PET::GLCM::Cluster shade	<0.0001	PET+CT::Fusion::Inverse difference	0.0182
PET::GLCM::Inverse difference moment	<0.0001	PET::GLCM::Cluster shade	0.0254
PET::Histogram::Entropy	0.0002		
PET::NGTDM::Contrast	<0.0001		
PET::Shape::Compactness	0.0204		
PET::GLCM::Difference entropy	<0.0001		
PET+CT::Fusion::Contrast	0.0499		
PET::GLCM::Dissimilarity	<0.0001		
PET::GLCM::Sum entropy	0.0049		
PET::GLZSM::Large zone high gray emphasis	<0.0001		
PET::GLZSM::Large zone size emphasis	0.0109		
PET::GLZSM::Zone size percentage	0.0197		
PET::NGTDM::Complexity	0.0002		
PET::NGTDM::Texture strength	<0.0001		

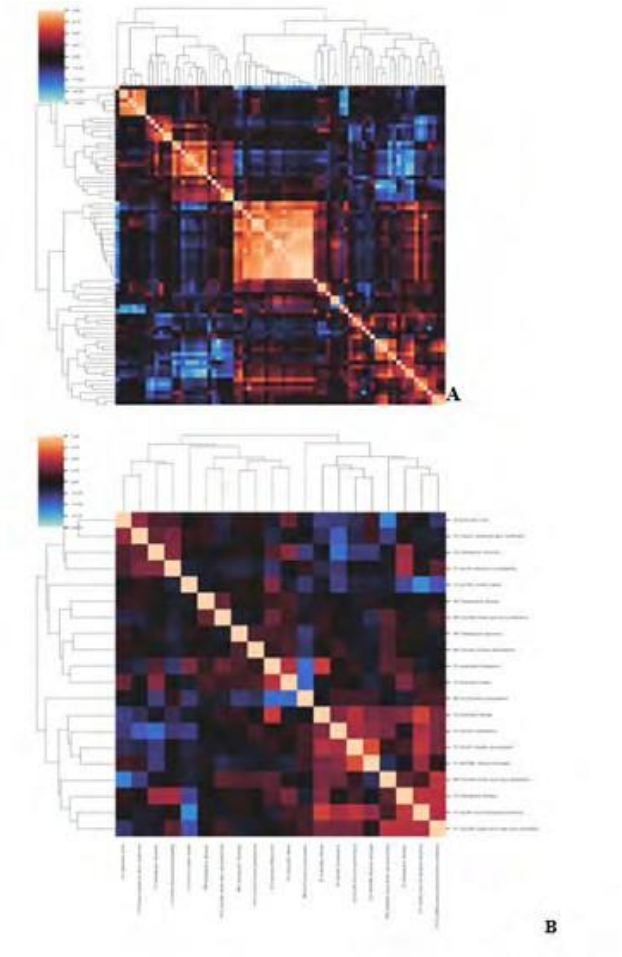

Figure 3: Correlation heat-map with radiomic features before (A) and after (B)redundancy reduction

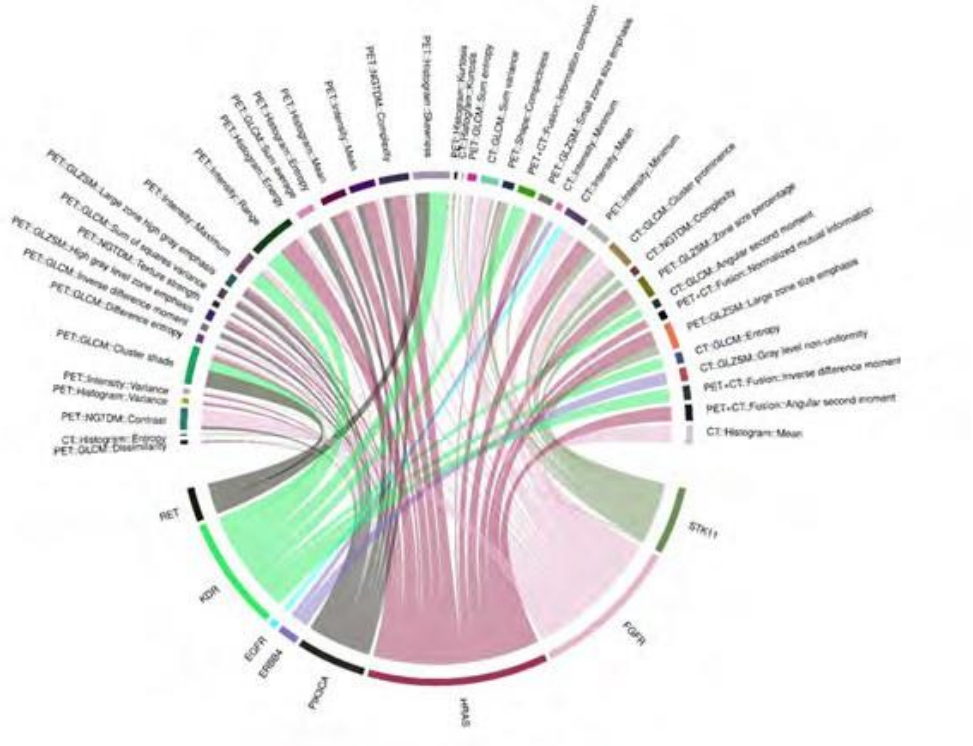

Figure 4: Chord plot of radiomic features associated with genetic mutations. Line width corresponds to the inverse p value

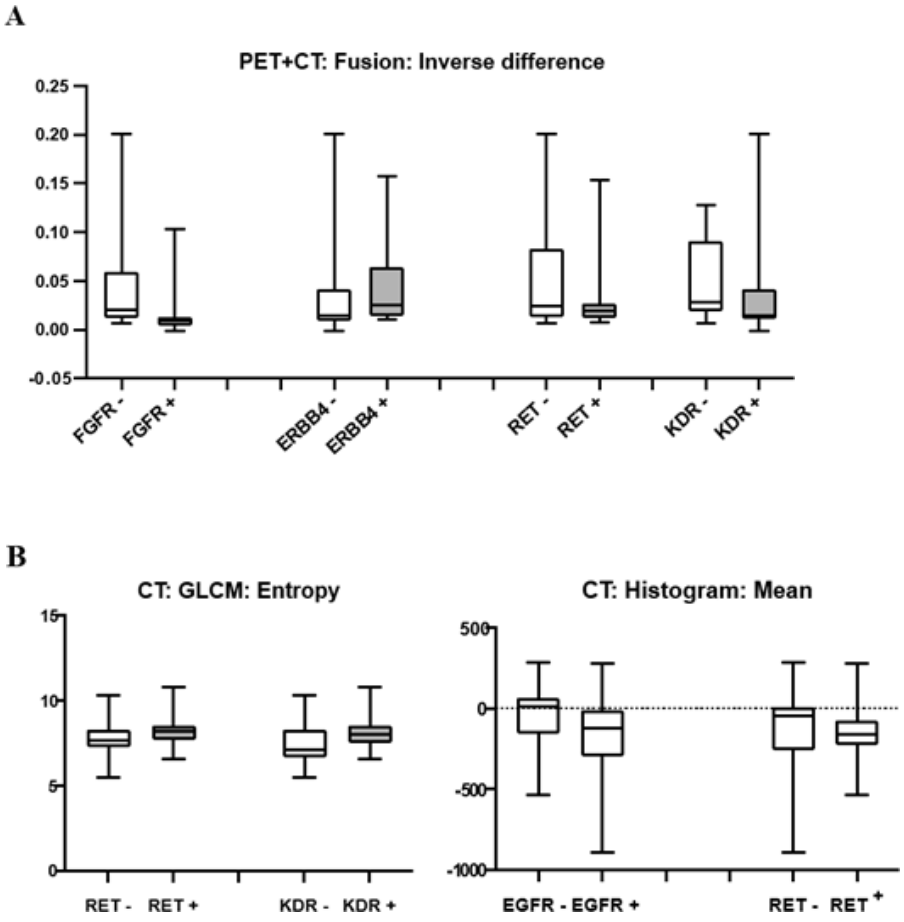

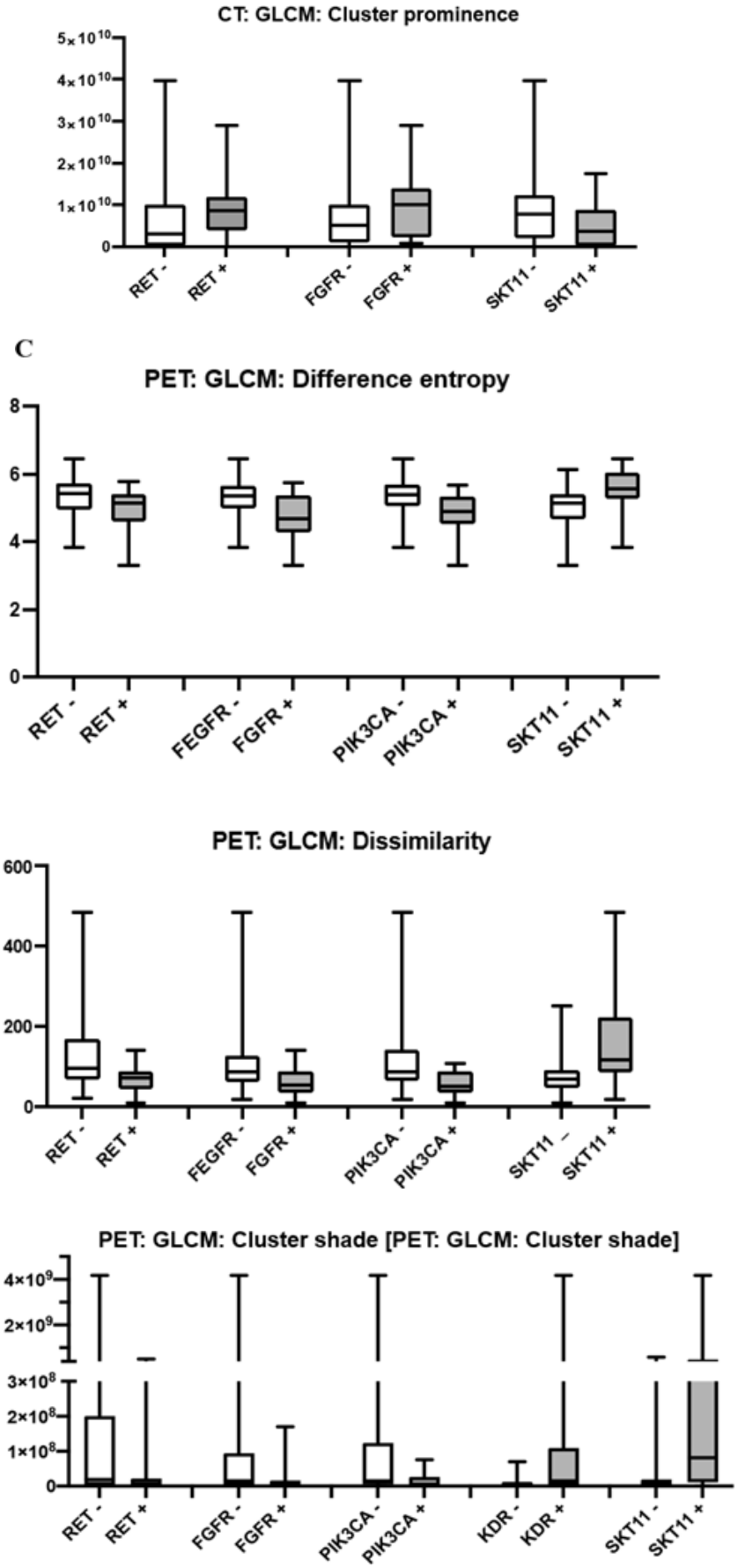

Figure 5: Box plots of the most sharing correlated features in PET-CT related radiomic(A) , CT-related radiomic features (B) and PET -related radiomics (C) with cfDNA mutations created in Graph-Pad Prism (P Value <0.05)

4.4 Radiomics to Predict Different Gene Mutations in Lung Cancer Patients: ROC analysis including AUC was done for radiomic features for prediction of mutation in a specific gene. (Table 2 Supplementary). The highest predictive value was observed in "CT::Histogram entropy", which predicted mutation in FGFR with AUC 0.886 and P<0.0001. FGFR and SKT11 showed the best AUCs as well as P-values in ROC analysis mostly with PET related features. Over all, CT-features had a high AUC for EGFR mutations (Figure 6/A), whereas PET features tended to have higher AUC for prediction of other mutations than CT features (Figure 4/B). PET GLCM cluster shade predicts mutation of RET, FGFR, PIK3CA and KDR with AUC 0.653, 0.7083, 0.732 and 0.682 respectively.

Table 2: IBSI-conform reporting of the study

Category	Details
Patient Preparation	
Volume of Interest	18F-FDG PET-positive lesions in the lung
Patient Preparation	Prior to imaging, patients fasted for 6 hours, blood sugar cutoff was 150 mg/dl
Radiotracer	18F-FDG
Acquisition and Reconstruction	
Scanner Type	Biograph™ TruePoint™ 64 (Siemens Healthineers, Erlangen, Germany)
18F-FDG PET	Static
Bed Position	5-6 bed position
Average Dose	300 MBq (range: 275-320 MBq) of 18F-FDG
Time After Injection	40-60 minutes after intravenous administration
Matrix Size (PET)	168x168
Slice Thickness (PET)	5mm
Iterations / Subsets	4 iterations, 21 subsets
Filter Type	3D FBP, Hamming filter 6.2mm cut-off
CT	Venous CE-CT
Injection	100 ml Iomeron 300 (Bracco, Milan Italy); rate of 2 ml/s; 50 ml saline flush
Matrix Size (CT)	512x512
Slice Thickness (CT)	3mm
Data Conversion	
Step 1	BQML PET voxel units transformed to weight-normalized SUV automatically by the Hermes Hybrid 3D software
Step 2	SUV PET voxel values transformed to tumor-to-background ratio (TBR) by dividing voxel values with mean of reference region (arcus aorta as cuboid VOI with 4ml volume)
Segmentation	
Software	Hermes Hybrid 3D ver 4.0.0
VOI Definition	Standard semi-automated iso-count 3D
Number of Experts	1+1 (1 nuclear medicine expert participated in independent delineations, followed by 1 senior nuclear medicine specialist for cross-validation and modification if necessary)
Reference Image	PET
Image / VOI Interpolation Method	Kriging interpolation in 3D, including nearest neighbors in distance of voxel size main diagonal (L, 2018)
Grid	Align by center
Extrapolation Beyond Original Image	Neighbor distance search calculated as original voxel size main diagonal + epsilon. Missing value: image minimum
Voxel Dimensions	1.0 x 1.0 x 1.0 mm and 4.0 x 4.0 x 4.0 mm (variable voxel resolution per feature as of reference (L, 2018))
Partially Masked Voxels (VOI)	Taken if more than half of original voxel area included
Discretization Method	Fixed bin width, variable number of bins
Bin Width	0.01 TBR and 0.1 TBR variable bin width per feature as of reference (L, 2018)
Image Biomarker Computation / Parameters	
Biomarker Set	Intensity features (6): Minimum, Maximum, Mean, Standard Deviation, Variance, Sum
	Histogram features (6): Energy, Entropy, Kurtosis, Mean, Skewness, Variance

	GLCM features (18): Inverse difference, Inverse difference moment, Sum average, Sum variance, Sum entropy, Difference variance, Difference entropy, Information correlation 2,
	Auto correlation, Cluster shade, Cluster prominence, Maximum probability, Entropy, Contrast, Dissimilarity, Angular second moment, Sum of squares variance, Correlation
	GLSZM features (11): Large zone emphasis, Small zone emphasis, Low grey level emphasis, High grey level emphasis, Small zone low grey level emphasis, Small zone high grey level emphasis,
	Large zone low grey level emphasis, Large zone high grey level emphasis, Grey level non-uniformity, Size zone non-uniformity, Zone percentage
	NGTDM (5): Coarseness, Contrast, Complexity, Busyness, Strength
	Morphological features (2): Volume (voxel counting), Compactness 1
Custom set	Morphological features (1): Spherical dice coefficient as of reference (L, 2018)
	Fusion features (GLCM features above a joint histogram) (14): Normalized Mutual Information, Angular second moment, Entropy, Contrast, Correlation, Dissimilarity, Sum of squares variance
	Inverse difference, Inverse difference moment, Information correlation 2, Auto correlation, Cluster shade, Cluster prominence, Maximum probability
Software	MUW radiomics engine . (L, 2018) Software availability upon reasonable request from the corresponding author.
Distance Weighting	No
CM Symmetry	Symmetric
CM / ZM Distance	Chebyshev distance 1
CM / ZM Aggregation	3D, full-merging

IBSI reporting structure of the study. The information presented herein is based on the Imaging Biomarker Standardization Initiative (IBSI) guidelines (L, 2018)

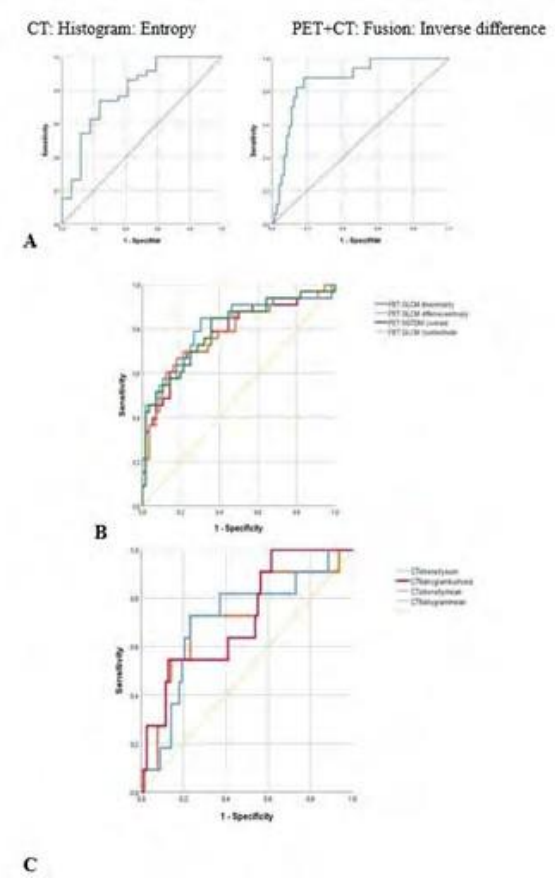

Figure 6: ROC analysis with calculation of AUC for FGFR related features (A), EGFR related features (B) and SKT11 related features (C). Analysis and curve production done by SPSS

Table 3: Calculated the area under curve (AUC)with 95% of CI (confidence interval), Specificity and sensitivity of each statistically correlated radiomic feature per mutated genes. Calculation done by Graph-Pad Prism.

Radiomic Feature/Mutation	Sensitivity %	Specificity %	AUC	P-Value
EGFR				
CT::Intensity::Mean	42.31	90.91	0.723	0.0167
CT::Histogram::Mean	43.59	90.91	0.723	0.0167
CT::Histogram::Kurtosis	43.5	90	0.717	0.0197
CT::Intensity::Sum	62.82	81.82	0.711	0.024
FGFR				
CT::Histogram::Entropy	52.94	91.67	0.8668	<0.0001
PET+CT::Fusion::Inverse difference	47.06	91.67	0.7933	0.0002
PET::GLZSM::Large zone high gray emphasis/FGFR	52.94	88.89	0.7312	0.0031
PET::GLCM::Inverse difference moment/FGFR	52.94	73.61	0.732	0.003
PET::GLCM::Sum average	70.59	65.28	0.7296	0.0034
PET::GLCM::Dissimilarity	47	88.89	0.7173	0.0055
PET::NGTDM::Texture strength	64.71	72.22	0.7165	0.0057
PET::GLCM::Cluster shade	47.06	80.56	0.7083	0.0078
PET::GLCM::Difference entropy	64.71	66.67	0.701	0.0102
PET::NGTDM::Complexity	52.94	80.56	0.6961	0.0122
PET::GLCM::Sum entropy	52.94	76.39	0.6887	0.0159
PET::NGTDM::Contrast	41.18	84.72	0.6585	0.0429
CT::GLCM::Cluster prominence	64.71	70.83	0.6565	0.0456
PIK3CA				
PET::Histogram::Entropy	76.19	63.24	0.7738	0.0002
PET::GLCM::Cluster shade	57.14	80.88	0.7234	0.0021
Radiomic Feature/Mutation	Sensitivity %	Specificity %	AUC	P-Value
PET::GLCM::Dissimilarity	52.38	86.76	0.7143	0.0031
PET::NGTDM::Texture strength	57.14	75	0.7052	0.0046
PET::GLCM::Difference entropy	71.43	60.29	0.6989	0.0061
PET::NGTDM::Contrast/PIK3CA	52.38	80.88	0.6898	0.0088
PET::GLZSM::Large zone high gray emphasis/PIK3CA	61.9	64.71	0.6758	0.0153
PET::NGTDM::Complexity/PIK3CA	61.9	70.59	0.6716	0.0179
PET::GLCM::Sum average	47.62	73.53	0.6604	0.0269
HRAS				
PET::Histogram::Skewness	62.22	70.45	0.6934	0.0017
PET+CT::Fusion::Normalized mutual information	76.09	62.79	0.6871	0.0024
PET::Histogram::Kurtosis	71.11	63.64	0.6773	0.004
PET::Histogram::Energy	75.56	63.64	0.6672	0.0066
CT::Intensity::Maximum	75.56	61.36	0.6601	0.0093
CT::Histogram::Energy	51.11	70.45	0.6566	0.011
CT::NGTDM::Texture strength	64.44	63.64	0.654	0.0123
PET::GLZSM::Small zone size emphasis	55.56	70.45	0.6513	0.014
CT::NGTDM::Coarseness	46.67	75	0.6303	0.0342
CT::GLZSM::Large zone low gray Emphasis	46.67	72.73	0.6253	0.0418
PET::GLZSM::Large zone size emphasis	57.78	70.45	0.6217	0.048
PET+CT::Fusion::Correlation	80	45.45	0.6212	0.0489
KDR				
PET::NGTDM::Busyness	98.65	98.65	0.9971	<0.0001

CT::GLCM::Angular second moment	75.68	66.67	0.6937	0.0185
PET+CT::Fusion::Inverse difference	60.81	73.33	0.6928	0.019
PET::GLCM::Cluster shade	63.51	73.33	0.6829	0.0261
Radiomic Feature/Mutation	Sensitivity %	Specificity %	AUC	P-Value
CT::GLCM::Entropy	50	66.67	0.682	0.0268
PET+CT::Fusion::Inverse difference moment	59.46	80	0.6739	0.0344
RET				
CT::Histogram::Kurtosis	83.78	67.31	0.7484	<0.0001
PET::NGTDM::Contrast	62.16	65.38	0.6996	0.0014
PET::GLCM::Dissimilarity	70.27	59.62	0.6959	0.0017
PET+CT::Fusion::Inverse difference	83.78	50	0.6939	0.0019
PET::GLCM::Inverse difference moment	78.38	50	0.6887	0.0025
CT::GLCM::Sum variance	86.49	53.85	0.6871	0.0027
PET::GLCM::Difference entropy	54.05	69.23	0.672	0.0059
PET::GLCM::Sum average	67.57	59.62	0.6679	0.0072
PET::GLCM::Sum of squares variance	70.27	53.85	0.6653	0.0081
CT::GLCM::Cluster prominence	81.08	50	0.6635	0.0088
PET::GLCM::Cluster shade	75.68	50	0.6538	0.0137
PET::GLZSM::High gray level zone emphasis	83.78	48.08	0.6585	0.0111
CT::GLCM::Entropy	72.97	55.77	0.6507	0.0158
PET::Histogram::Variance	78.38	48.08	0.6497	0.0165
PET::Histogram::Mean	65.79	60.78	0.6434	0.0211
PET::Intensity::Maximum	70.27	59.62	0.6403	0.0246
PET::Intensity::Mean	56.76	65.38	0.6273	0.0414
CT::Histogram::Mean	70.27	67.31	0.6273	0.0414
CT::Intensity::Sum	72.97	50	0.6253	0.0448
ERBB4				
PET+CT::Fusion::Inverse difference	72	56.25	0.6513	0.0272
CT::NGTDM::Coarseness	44	68.75	0.6394	0.0418
SKT11				
PET::GLCM::Dissimilarity	84.85	67.86	0.8095	<0.0001
PET::NGTDM::Contrast	84.85	64.29	0.7949	<0.0001
PET::GLCM::Cluster shade	78.79	60.71	0.7803	<0.0001
PET::GLCM::Inverse difference moment	60.61	87.5	0.7727	<0.0001
PET::GLCM::Difference entropy	60.61	83.93	0.7749	<0.0001
PET::GLZSM::Large zone high gray emphasis	60.61	80.36	0.7597	<0.0001
PET::NGTDM::Texture strength	62.5	80.7	0.7516	<0.0001
PET::Histogram::Entropy	63.64	80.36	0.7348	0.0002
PET::NGTDM::Complexity	60.61	80.36	0.7348	0.0002
CT::Histogram::Entropy	69.7	60.71	0.6851	0.0037
PET::GLCM::Sum entropy	72.73	60.71	0.678	0.0052
CT::GLCM::Sum variance	60.61	66.07	0.6721	0.0069
PET::GLZSM::Large zone size emphasis	50	75	0.6629	0.0113
PET::GLZSM::Zone size percentage	72.73	53.57	0.648	0.0202
PET::Shape::Compactness	81.82	41.07	0.6472	0.0209
CT::GLCM::Cluster prominence	72.73	48.21	0.6488	0.0195
PET+CT::Fusion::Contrast	60.61	66.07	0.625	0.0497

4.5 Decision Tree predictive Model: Similar to a recently published study, we tested for a predictive model according to our results (Ceriani, 2021). In this decision tree model for each mutation the two correlated features with the highest AUC were determined. Using ROC analysis with Youden index we determined thresholds for each of the features and categorized lesions according to this value as 0 (lesion is not beyond the score with regard to gene mutation) and 1 (lesion is beyond the score with regard to gene mutation). Patients were then divided into 3 groups according to the scoring: Score zero (both features with value 0), score one (one of the two features with value 1) and score 2 (both features with value 1). For EGFR mutation 'CT::Intensity::Mean' and 'CT::Histogram::Mean' were considered for the predictive model and the prevalence of mutations increased from 0% (0/5) for score 0 to 84% (21/25) in score 1 and 91% (21/23) in score 2. FGFR mutation was considered with 'PET+CT::Fusion::Inverse difference' and 'CT::Histogram::Entropy'. The prevalence of mutations increased from 5% to 50% and 90% for score zero, one and two respectively. For HRAS mutation combination of 'PET::Histogram::Skewness' and 'PET+CT::Fusion::Normalized mutual information' , resulted the increasing prevalence of mutation from 8% to 83% and 87% (Score zero, one and two respectively). In RET mutation the concordance of 'PET::NGTDM::Contrast' and 'CT::Histogram::Kurtosis', resulted a prevalence of mutation from 0% in group with score zero to 78% for score 1 and 83% for score 2. For PIK3CA two PET related parameters 'PET::GLCM::Cluster shade' and 'PET::GLCM::Dissimilarity' had the best AUC and prevalence of mutation increased from 12% to 46% and 62% for score zero, one and two respectively. Finally SKT11 mutation also considered with two PET parameters 'PET::GLCM::Dissimilarity' and 'PET::NGTDM::Contrast'. The prevalence of mutation increased from 17% in the group with score zero to 53% in group with score 1 and 66% in group with score 2.

5. Discussion

In this pilot study, we prospectively aimed to correlate liquid biopsies with radiomics. Radiomic features are capable of representing tumor phenotypes - especially PET-based radiomics- because of the underlying mechanism of action. (Grossmann, 2017) (Xiong, 2018). Such an approach can support progress in personalized medicine as a feasible and non-invasive tumor characterization. Another important possibility of this strategy would be the capability for better clarification of tumor heterogeneity which might lead to a better decision making in targeted tumor therapy. (Lian, 2016) We choose lung cancer for this first pilot study, because it is still the most common cause of cancer death worldwide (Sung, 2012). The use of liquid biopsy in clinical practice was suggested for EGFR analysis in NSCLCs even since 2004 (Tu, 2016). Consequently, more data are available –especially regarding EGFR- for comparison and interpretation (Wang Z. , 2018) (Deng, 2020). In a recently published study genome profiling of cfDNA, which was done for colon cancer patients (similar to our study, patients were in different stage of disease), they had a high concordance with tissue biopsy results, when the time between obtaining the two biopsies was less than 30 days (Lan, 2021) (Cervena, 2021). In our study we observed the same results for EGFR mutation: In patients which liquid biopsy was done parallel or in short time duration after/before tissue biopsy (7 patients), the EGFR mutation results was similar to tissue biopsy.

Our study shows a significant correlation between tumor volume and TLG measured with PET/CT and mortality of lung cancer which is in concordance with similar study on cfDNA in lung and breast cancer patients. (Bredno, 2021) Few studies tried to find the concordance of circulation DNA/RNA with tissue biopsy and / or its correlation with radiomic features (Veldore, 2018) (Guibert, 2020): Dama et al reported several studies which used mi-RNA as a diagnostic biomarker in circulating blood of lung cancer patients and tried to correlate it with CT features. They reported a sensitivity range between 75-78%. Looking into the literature it is evident, that almost all mutations show higher prevalence in liquid biopsy than tissue biopsy; as an example the prevalence of EGFR mutation in tissue biopsies of lung cancer patients ranged between 20%46% (Gejman, 2019) (Aye, 2021) (Gahr, 2013) (YL, 2016), whereas in liquid biopsies the prevalence ranged between 64%-85% (Singh, 2017). In our study population, 72% of patients had EGFR mutation which is in concordance with other studies (Su, 2018). The reason of this higher prevalence in cfDNA is probably due to the higher capability of mutated cells for invasion and reaching into the blood circulation compared to non-mutated ones, which is one important advantage of cfDNA for detection of different tumor sub-populations. Furthermore, biopsy is prone to sampling errors due to spatial and temporal tumor heterogeneity. In terms of mutation prediction, EGFR mutation could be predicted mainly with CT-related radiomic-features rather than PET whereas FGFR and SKT-11 could be predicted with the highest AUC P-Values with PET- related features (Figure 6). Correlation studies of PET/CT radiomic and EGFR mutation were mainly done with tissue biopsies; in many of them it has been shown that EGFR mutation is mostly correlated with shape, compactness and overall physical characteristics of the tumor/metastasis. (Yip, 2017) (Zhang, 2020) Most studies in cfDNA of lung cancer patients focused on one – for example only

EGFR- or maximally two or three important mutations (EGFR and KRAS or FGFR and ALK) as the most common well-known mutations in lung cancer - and their sensitivity and specificity on early diagnosis, estimation of prognosis, therapy response or recurrence of NSCLC (Filipska, 2021). One strength of our study is that we used a panel of genome assays including 50 important oncogenes that can provide an overview of all activated oncogenic pathways which may be reflected by radiomics. In our study due to the low percentage of mutated cases we could not check the correlation of

radiomic features with KRAS. One study using cfDNA reports its prevalence up to 50%, whereas others showed lower rates (Boldrin, 2020) (Zulato, 2020). On the other hand, there are studies, which pronounced the importance of cfDNA extraction methods, and /or mutation detection packages, which significantly lead to increasing false negativity rather than false positivity in mutation tests -specially for KRAS- (Garzón, 2016). Instead of KRAS, we have got a profound correlation of Radiomics with mutated HRAS patients as another important oncogene from RAS family.

In our study KDR (KDR also is known as VEGFR 2), FGFR, PIK3CA and especially RET showed a high percentage of mutation. They are all together important members of the TK-pathway, which is the most important therapy target in NSCLC patients . (Liu, 2017) (Yamaoka, 2018) PIK3CA is reported to be highly mutated in both SCC and ADC tissue samples -but more in SCC- (Campbell, 2016) which is in concordance which our liquid biopsy results. In a recently published retrospective study which combined FGFR mutation detection in cfDNA and tissue biopsies the prevalence of FGFR mutation in different types of lung cancer patients was about 2% which was significantly higher in SCC patients. (Zhou, 2021) . In this study more than half samples – whether cfDNA or tissue – which were positive for FGFR mutation have had also PIK3CA or PIK3R2 mutation in cfDNA samples showing the activation of TK pathway in these patients. In our study we observed FGFR mutation in about 10 % of patients and PIK3CA mutation in about 38% of patients (Figure 2). Both had more correlations with PET features rather than CT and more than half of correlated PET features were similar together. (Table 2)

VEGFR-2 (KDR) and RET-targeting drugs are novel anti-tumor therapies and are important for angiogenesis and invasion of the tumor. (Yan Zhou, 2015) In one study on ADC patients with tissue biopsy assay, EGFR is considered as a driver mutation which occurred primarily and in high frequency but other mutations -like KDR- are branching private mutations which occur later on and in individuals with highly heterogenous ADC. (Pelosi, 2016). In a review the prevalence of RET mutation ,as a tumor diver gene, was about 1.2%-6% and more common in ADC. (R, 2013). RET mutated lung tumors were significantly more invasive and less differentiated in comparison to EGFR or ALK mutated ones. (Joshua D. Campbell, 2016) (Qiu, 2020) (Li, 2019) This may explain the higher prevalence of its mutation in cfDNA than reported in tissue biopsies: RET and VEGF mutated cells are more invasive and reach easily to the circulation. Interestingly, RET, KDR and FGFR are significantly correlated with “PET CT fusion inverse difference” which is one of the representative features of tumor heterogeneity in FDG uptake (PET) as well as HU Unit (CT). According to (Figure 3) the more heterogenic the tumor uptake or tumor structure is, the higher is the likelihood of mutations in RET, KDR and FGFR.

The percentage of mutations in other important genes in lung cancer -especially tyrosine kinase pathway- like SKT11 was, as expected, higher than reported in tissue biopsy studies (Figure 2) (Facchinetti, 2017). In the published cfDNA mutation assays we didn’t find any available study, which investigated mutations of SKT11 in lung cancer patients. SKT11, FGFR & PIK3CA together with RET mutation had the highest connection to each other in terms of correlation with different features. Unlike the tumor driver mutations, SKT11 as a tumor suppressor gene, shows to be more mutated when tumors are more homogenous. (Figure5 A, B and C) This points towards an increasing tumor heterogeneity by an activation of the TKpathway via EGFR or other driver oncogenes rather than mutations of a tumor suppressor gene. An important limitation of tissue biopsy is its incapacitation for evaluation and clarifying of tumor heterogenicity. Most malignancies, especially NSCLC, present as a heterogenetic entity with multiple sub–populations. Characterization of this sub-population is essential in personalized medicine. (Voigt, 2020) Combination of liquid biopsy and radiomics has the potential to connect the phenotypical heterogeneity to the genome heterogeneity of tumors and to improve tumor characterization. (Jr, 2018). In the aspect of correlation with the radiomics, in our study 66.7% (30 from 45) of all correlated radiomic-features were PET –related features or fusion PET/CT related ones, which points towards that mutations more often affect tumor metabolism rather than morphological features. Recently deep learning and machine learning systems emerged for the prediction of mutations based on radiomics in different tumors, which were shown to provide highly performant predictive models (Le, 2021). Because of a low sample size, it was not useful to test machine-learning systems; nevertheless, our AUC results are completely comparable to those studies, which employed ML for the detection of EGFR status. We had AUC > 0.7 with 95% CI (confidence interval) for all correlated features, which is comparable to Wang et al. (Wang S. , 2019) (Yin, 2021). So far, a rather comprehensive gene mutation assay on cfDNA (50 genes) wasn’t performed in lung cancer patients in combination with F-18 FDG PET-CT radiomics. Therefore, interpretation of the sensitivity of our cfDNA mutation assay is not possible due to a lack of comparable studies. Our findings lay the basis for further evaluations and for a further improvement of this strategy. Despite our low sample size, multi-parametric radiomic based models seem to be a useful approach that can be used to estimate the activation of special cascades in the tumor cells. Our next ongoing step is to extend our sample size not only in lung cancer patients but also in other solid tumors and using possible machine learning workflows for better characterization of activated cascades. Parallel it is important to modify extraction methods for increasing the sensitivity of mutation results.

6. Acknowledgements

The financial support by the Austrian Federal Ministry for Digital and Economic Affairs, the National Foundation for Research,

Technology and Development and the Christian Doppler Research Association is gratefully acknowledged. This research was also funded by Siemens Healthineers.

References

1. Alvarez JV. Oncogene pathway activation in mammary tumors dictates FDG-PET uptake. Cancer Res. 2014;74(24):7583–98.
2. Aye PS. Population-based incidence rates and increased risk of EGFR mutated non-small cell lung cancer in Māori and Pacifica in New Zealand. PLOS ONE. 2021, May 7.
3. Bi F. Circulating tumor DNA in colorectal cancer: opportunities and challenges. 2020;12(3):1044–1055.
4. Boldrin E. Detection of loss of heterozygosity in cfDNA of advanced EGFR- or KRAS-mutated non-small-cell lung cancer patients. Int J Mol Sci. 2020;66.
5. Boysen AK. Cell-free DNA levels and correlation to stage and outcome following treatment of locally advanced rectal cancer. Tumor Biol. 2017.
6. Boysen AK. Cell-free DNA levels and correlation to stage and outcome following treatment of locally advanced rectal cancer. Tumor Biol. 2017.
7. Boysen AK. Cell-free DNA levels and correlation to stage and outcome following treatment of locally advanced rectal cancer. Tumor Biol. 2017.
8. Boysen AK. Cell-free DNA levels and correlation to stage and outcome following treatment of locally advanced rectal cancer. Tumor Biol. 2017.
9. Boysen AK. Cell-free DNA levels and correlation to stage and outcome following treatment of locally advanced rectal cancer. Tumor Biol. 2017.
10. Bredno J. Clinical correlates of circulating cell-free DNA tumor fraction. PLOS ONE. 2021.
11. Campbell JD. Distinct patterns of somatic genome alterations in lung adenocarcinomas and squamous cell carcinomas. Nat Genet. 2016.
12. Ceriani L. Radiomics analysis of [18F]-fluorodeoxyglucose-avid thyroid incidentalomas improves risk stratification and selection for clinical assessment. Thyroid. 2021;31(1):88–95.
13. Cervena K. Mutational landscape of plasma cell-free DNA identifies molecular features associated with therapeutic response in patients with colon cancer: A pilot study. Mutagenesis. 2021, July.
14. Cohen JD. Combined circulating tumor DNA and protein biomarker-based liquid biopsy for the earlier detection of pancreatic cancers. Proc Natl Acad Sci U S A. 2017;114(38):10202–7.
15. Deng Q. Detection of plasma EGFR mutations for personalized treatment of lung cancer patients without pathologic diagnosis. Cancer Med. 2020, March 9;9(6):2085–2095.
16. Facchinetti F. LKB1/STK11 mutations in non-small cell lung cancer patients: Descriptive analysis and prognostic value. Lung Cancer. 2017;112:62–8.
17. Filipska M. Mutated circulating tumor DNA as a liquid biopsy in lung cancer detection and treatment. Mol Oncol. 2021;15(6):1667–82.
18. Gahr S. EGFR mutational status in a large series of Caucasian European NSCLC patients: Data from daily practice. Br J Cancer. 2013;1821–8.
19. Garzón M. KRAS mutations in the circulating free DNA (cfDNA) of non-small cell lung cancer (NSCLC) patients. Transl Lung Cancer Res. 2016;5(5):511–6.
20. Gejman R. Prevalence of EGFR mutations and clinico-pathological characteristics of Chilean lung cancer patients. 2019;20(1):1–4.
21. Grossmann P. Defining the biological basis of radiomic phenotypes in lung cancer. eLife. 2017.
22. Guibert N. Current and future applications of liquid biopsy in non-small cell lung cancer from early to advanced stages. Eur Respir Rev. 2020.
23. Heiden BT. 18F-FDG PET intensity correlates with a hypoxic gene signature and other oncogenic abnormalities in operable non-small cell lung cancer. PLOS ONE. 2018.
24. Herbreteau G. Circulating free tumor DNA in non-small cell lung cancer (NSCLC): Clinical application and future perspectives. J Thorac Dis. 2019.
25. Hong D. Radiomics signature as a predictive factor for EGFR mutations in advanced lung adenocarcinoma. Front Oncol. 2020.
26. Ianza A. EGFR mutation analysis on circulating free DNA in NSCLC: A single-center experience. J Cancer Res Clin Oncol. 2021.
27. Im HJ. Usefulness of combined metabolic–volumetric indices of 18F-FDG PET/CT for the early prediction of neoadjuvant chemotherapy outcomes in breast cancer. Nucl Med Mol Imaging. 2013;47:36–43.
28. Martins I. Liquid biopsies: Applications for cancer diagnosis and monitoring. Genes (Basel). 2021;349.
29. Campbell JD. Distinct patterns of somatic genome alterations in lung adenocarcinomas and squamous cell carcinomas. Nat Genet. 2016.
30. Jr JD. Liquid biopsy and its role in an advanced clinical trial for lung cancer. Exp Biol Med. 2018;243(3):262–71.
31. Kabir Z. Sex-differences in lung cancer cell-types? An epidemiologic study in Ireland. Ulster Med J. 2008;77(1):31–5.
32. Lan YT. High concordance of mutation patterns in 10 common mutated genes between tumor tissue and cell-free DNA in metastatic colorectal cancer. Am J Cancer Res. 2021;11(5):2228–37.
33. Le NQ. Machine learning-based radiomics signatures for EGFR and KRAS mutations prediction in non-small-cell lung cancer. Int J Mol Sci. 2021;22(17).
34. Li AY. RET fusions in solid tumors. Cancer Treat Rev. 2019.
35. Lian C. Selecting radiomic features from FDG-PET images for cancer treatment outcome prediction. Med Image Anal. 2016.
36. Liu TC. Role of epidermal growth factor receptor in lung cancer and targeted therapies. Am J Cancer Res. 2017;7(2):187–202.

37. Liu HE. Detection of EGFR mutations in cfDNA and CTCs, and comparison to tumor tissue in non-small-cell lung-cancer (NSCLC) patients. Front Oncol. 2020.
38. Lyskjær I. Correlation between early dynamics in circulating tumour DNA and outcome from FOLFIRI treatment in metastatic colorectal cancer. Sci Rep. 2019.
39. Ma X. Cell-free DNA provides a good representation of the tumor genome despite its biased fragmentation patterns. PLOS ONE. 2017.
40. Ma X. Cell-free DNA provides a good representation of the tumor genome despite its biased fragmentation patterns. PLOS ONE. 2017.
41. Ma X. Cell-free DNA provides a good representation of the tumor genome despite its biased fragmentation patterns. PLOS ONE. 2017.
42. Ntzifa A. Detection of EGFR mutations in plasma cfDNA and paired CTCs of NSCLC patients before and after osimertinib therapy using crystal digital PCR. Cancers. 2021.
43. Pavlova NN. The emerging hallmarks of cancer metabolism. Cell Metab. 2016;23(1):27–47.
44. Pelosi G. Deciphering intra-tumor heterogeneity of lung adenocarcinoma confirms that dominant, branching, and private gene mutations occur within individual tumor nodules. Virchows Arch. 2016.
45. Qiu Z. Unique genetic characteristics and clinical prognosis of female patients with lung cancer harboring RET fusion gene. Nat Commun. 2020.
46. R G. New targetable oncogenes in non–small-cell lung cancer. J Clin Oncol. 2013.
47. Remon J. Liquid biopsy in oncology: A consensus statement of the Spanish Society of Pathology and the Spanish Society of Medical Oncology. Clin Transl Oncol. 2020;823–34.
48. Sagerup CM. Sex-specific trends in lung cancer incidence and survival: A population study of 40,118 cases. BMJ. 2011;66:301–7.
49. Singh AP. Circulating DNA in EGFR-mutated lung cancer. Ann Transl Med. 2017;5(18):379.
50. Siravegna G. How liquid biopsies can change clinical practice in oncology. Ann Oncol. 2019;1580–90.
51. Su K-Y. Mutational monitoring of EGFR T790M in cfDNA for clinical outcome prediction in EGFR-mutant lung adenocarcinoma. PLOS ONE. 2018.
52. Sung H. Global Cancer Statistics 2020: GLOBOCAN Estimates of Incidence and Mortality Worldwide for 36 Cancers in 185 Countries. 2020;71(3):209–249.
53. Tu M. Liquid Biopsy for Detection of Actionable Oncogenic Mutations in Human Cancers and Electric Field Induced Release and Measurement Liquid Biopsy (eLB). Analyst. 2016;141(2):393–402.
54. Veldore VH. Validation of liquid biopsy: plasma cell-free DNA testing in clinical management of advanced non-small cell lung cancer. Lung Cancer: Targets and Therapy. 2018.
55. Verma M. Genome-wide association studies and epigenome-wide association studies go together in cancer control. Future Oncology. 2016;12(13).
56. Verma M. Genome-wide association studies and epigenome-wide association studies go together in cancer control. Future Oncology. 2016;12(13).
57. Verma M. Genome-wide association studies and epigenome-wide association studies go together in cancer control. Future Oncology. 2017;1645–1664.
58. Voigt W. Beyond tissue biopsy: a diagnostic framework to address tumor heterogeneity in lung cancer. Curr Opin Oncol. 2020;32(1):68–77.
59. Volik S. Cell-free DNA (cfDNA): Clinical Significance and Utility in Cancer Shaped by Emerging Technologies. Molecular Cancer Research. 2016.
60. Wang S. Predicting EGFR mutation status in lung adenocarcinoma on computed tomography image using deep learning. Lung Cancer and Imaging. 2019.
61. Wang Z. Detection of EGFR mutations in plasma circulating tumor DNA as a selection criterion for first-line gefitinib treatment in patients with advanced lung adenocarcinoma (BENEFIT): a phase 2, single-arm, multicenter clinical trial. Clinical Trial. 201
62. Xiong J. The role of PET-based radiomic features in predicting local control of esophageal cancer treated with concurrent chemoradiotherapy. Scientific Reports. 2018.
63. Yamaoka T. Receptor Tyrosine Kinase-Targeted Cancer Therapy. Int J Mol Sci. 2018;19(11):3491.
64. Zhou Y. The multi-targeted tyrosine kinase inhibitor vandetanib plays a bifunctional role in non-small cell lung cancer cells. Sci Rep. 2015.
65. Yin G. Prediction of EGFR mutation status based on 18F-FDG PET/CT imaging using deep learning-based model in lung adenocarcinoma. Front Oncol. 2021.
66. Yip SS. Associations between somatic mutations and metabolic imaging phenotypes in non-small cell lung cancer. J Nucl Med. 2017;58(4):569–576.
67. YL Z. The prevalence of EGFR mutation in patients with non-small cell lung cancer: a systematic review and meta-analysis. Oncotarget. 2016; 7:78985–78993.
68. Zhang M. Performance of 18F-FDG PET/CT radiomics for predicting EGFR mutation status in patients with non-small cell lung cancer. Front Oncol. 2020; 10:568857.
69. Zhou Z. Targeting FGFR in non-small cell lung cancer: implications from the landscape of clinically actionable aberrations of FGFR kinases. Cancer Biol Med. 2021;18(2):490–501.
70. Zulato E. Early assessment of KRAS mutation in cfDNA correlates with risk of progression and death in advanced non-small-cell lung cancer. British Journal of Cancer. 2020; 123:81–91.